



e-ISSN: 2319-8753 | p-ISSN: 2320-6710

# IJIRSET

International Journal of Innovative Research in  
**SCIENCE | ENGINEERING | TECHNOLOGY**

# INTERNATIONAL JOURNAL OF INNOVATIVE RESEARCH

IN SCIENCE | ENGINEERING | TECHNOLOGY

Volume 10, Issue 6, June 2021

**ISSN** INTERNATIONAL  
STANDARD  
SERIAL  
NUMBER  
INDIA

**Impact Factor: 7.512**

9940 572 462

6381 907 438

[ijirset@gmail.com](mailto:ijirset@gmail.com)

[www.ijirset.com](http://www.ijirset.com)

# Complete X-ray Peak Profile Analysis of $\text{Co}_x\text{Zn}_{0.95-x}\text{Cr}_{0.05}\text{O}$ nanoparticles based on Williamson–Hall and SSP Methods

Supriya Balsure<sup>1\*</sup>, Vikram More<sup>2</sup>, Sanskruti Kadam<sup>3</sup>, Dilip Kulkarni<sup>4</sup>, Yogiraj Vijapure<sup>5</sup>,  
Ankush Kadam<sup>6</sup>

Research Student, Department of Physics, Jawahar Mahavidyalaya, Anadur, Osmanabad (M.S.) India<sup>1</sup>

Research Student, Department of Physics, Rajarshi Shahu College, Pathri, Dist. Aurangabad (M.S.) India<sup>2</sup>

Research Student, Department of Physics, Shrikrishna Mahavidyalaya, Gunjoti, Dist. Osmanabad (M.S.) India<sup>3</sup>

Professor, Department of Chemistry, Shrikrishna Mahavidyalaya, Gunjoti, Dist. Osmanabad (M.S.) India<sup>4</sup>

Associate Professor, Department of Chemistry, Shrikrishna Mahavidyalaya, Gunjoti, Dist. Osmanabad (M.S.) India<sup>5</sup>

Research Guide, Department of Physics, Jawahar Mahavidyalaya, Anadur, Osmanabad (M.S.) India<sup>6</sup>

**ABSTRACT:**  $\text{Co}_x\text{Zn}_{0.95-x}\text{Cr}_{0.05}\text{O}$  nanoparticles of dilute magnetic semiconductor (DMS) were obtained by using sol-gel auto-combustion route. Powder X-ray diffraction technique was adopted to study the crystallography and strain mechanism induced in the crystal lattice. XRD patterns of all the samples confirm the single phase wurtzite type crystal structure without any impurity phase. Addition of isovalent transition metal  $\text{Co}^{2+}$  ions in Zn-Cr crystal decreases the lattice parameter ‘a’ and ‘c’. Average crystallite and lattice strain induced in the crystal lattice was estimated by using the Williamson – Hall (W-H) and strain size plot (SSP) methods. Three different models Uniform deformation model (UDM), uniform stress deformation model (UDEM) and uniform deformation energy density model (UEDDM) were assumed for W-H analysis. Crystallite size obtained from another strain – size plot (SSP) method found in the range 19.32 to 25.60 nm and decreasing tensile type strain is induced in the crystal lattice which is in good agreement with the results obtained from W-H analysis.

**KEYWORDS:** Sol-gel synthesis, crystallite size, W-H analysis, strain size plot method

## I. INTRODUCTION

Fabrications of nanostructured materials for particular application have attracted much attention of the researchers in the recent years. Nanomaterials show unusual physical and chemical properties over the bulk counterpart due to their large surface to volume ratio [1-3]. Dilute magnetic semiconductors (DMS), particularly transition metal doped zinc oxides are the subject of extensive research due to their fascinating structural, magnetic and optical properties [4]. Zinc oxide at room temperature possesses semiconducting behaviour with wide energy band gap (3.35 eV) and high excitation binding energy (60 meV) [2]. Semiconducting materials with improved optoelectronic properties, cost-effective and lightweight are gained prime importance and zinc oxide is one of the most useful materials. ZnO is one of the II-VI semiconducting materials possessing hexagonal wurtzite crystal geometry. Previous studies shows that the transition metal (TM) doped zinc oxide nanostructures have been comprehensively studied [5-9].

Synthesis routes and synthesis conditions and selection of proper dopant can control the physical properties of ZnO nanostructures such as shape and size of the material, magnetic, optical and electrical properties. Substitution of higher magnetic ion in ZnO lattice improves the magnetic behaviour of the doped samples. Based on desired applications, several synthesis routes have been developed in order to obtain the pure and doped ZnO nanoparticles which includes solvothermal, hydrothermal, sol-gel, sonochemical, chemical co-precipitation [10-12]. Among these, sol-gel synthesis route is one of the best methods to produce the DSM's nanoparticles at large scale. This method has some advantages over the other synthesis approaches such as cost effective and relatively low temperature synthesis. Microstructural analysis is one of the most important properties of the nanomaterials which originate mainly due to the atomic

rearrangements in the crystal lattice after doping of other elements. These atomic rearrangements induce an intrinsic strain within the crystal lattice which in turn changes the microstructural properties. The substitution of TM ion in ZnO crystal lattice, due to its ionic radii difference, generates some defects within the crystal lattice which in turn influences the optical and magnetic properties [13-15]. Hence study of microstructural properties gets prime importance in order to understand the physical properties of ZnO nanoparticles. X-ray line broadening's clearly indicates the size and strain effect induced in the crystal lattice. X-ray peak profile analysis is one of the methods which provide the information of strain induced in the crystal lattice and other microstructural properties. Numerous methods have been developed to investigate the microstructural properties of nanoparticles by using X-ray peak profile analysis, such as Williamson-Hall (W-H), size – strain plot (SSP), Halder-Wagner (H-W), Nelson-Relay (N-R) etc [16-18].

In the present investigation, we have synthesized the  $\text{Co}^{2+}$  doped Cr-Zn-O nanoparticles via sol-gel auto-combustion technique. All the samples were characterized by powder X-ray diffraction patterns. W-H and SSP methods have been adopted for the size and strain analysis of the samples by using X-ray line broadenings. Uniform deformation model (UDM), uniform stress deformation model (USDM) and uniform deformation energy density model were assumed for the W-H analysis and the results were compared with SSP method.

## II. METHODOLOGY

Oxide nanoparticles of  $\text{Co}_x\text{Zn}_{0.95-x}\text{Cr}_{0.05}\text{O}$  ( $x = 0.0, 0.02, 0.04, 0.06, 0.08$  and  $0.1$ ) were produced by using sol-gel auto-ignition process. High purity (>98.5%) metal nitrates  $\text{Co}(\text{NO}_3)_2 \cdot \text{H}_2\text{O}$ ,  $\text{Zn}(\text{NO}_3)_2 \cdot \text{H}_2\text{O}$ ,  $\text{Cr}(\text{NO}_3)_3 \cdot \text{H}_2\text{O}$  and citric acid were used as raw materials. Deionized double distilled water was used to dissolve the raw materials with their weight proportion. The mixed solution was continuously stirred by maintaining the constant temperature of  $90^\circ\text{C}$ . Citric acid, as a chelating agent, was mixed in the nitrates solution with the ratio of 1:3 of metal nitrate to citrate. The pH of the solution was kept constant at 7 by slowly adding the liquid ammonia in the solution. Continuous stirring at constant pH and temperature for 2 to 3 hours converts the solution into viscous gel. After half an hour the dark brown gel was burnt by self – ignition process and converted into brown ash. The grinded ash powders were sintered at  $900^\circ\text{C}$  for 6 hours in order to obtain the final products. The as-prepared samples were characterized by X-ray diffraction technique for their structural investigations. Powder X-ray diffraction technique was adopted to obtain the XRD patterns at room temperature within the  $2\theta$  range of  $20^\circ$  to  $80^\circ$ . All the XRD patterns were recorded on Regaku (Miniflux II) diffractometer with  $\text{Cu-K}\alpha$  radiation ( $1.5406 \text{ \AA}$ ) operated at 40 kV.

## III. RESULTS AND DISCUSSION

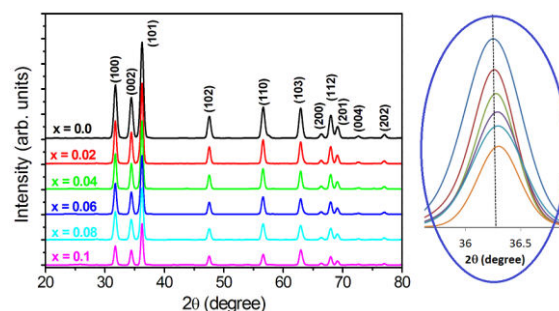


Fig. 1: X-ray diffraction patterns of  $\text{Co}_x\text{Zn}_{0.95-x}\text{Cr}_{0.05}\text{O}$  nanoparticles (left) and expanded (101) peak (right)

Powder X-ray diffraction patterns of  $\text{Co}_x\text{Zn}_{0.95-x}\text{Cr}_{0.05}\text{O}$  ( $x = 0.0, 0.02, 0.04, 0.06, 0.08$  and  $0.1$ ) recorded at room temperature are given in Figure 1 (Left panel). Bragg's reflections occurred for the planes (100), (002), (101), (102), (110), (103), (200), (112), (201), (004), and (202) confirm the hexagonal wurtzite structure corresponding to the space group  $\text{P6}_3\text{mc}$ . No any un-indexed reflection peak is observed which implies that all the samples possess single phase. Right panel of Figure 1 shows the expanded view of most intensive plane (101) which clearly shows that peak height decreases and peak position shifted slightly towards higher angles with the addition of  $\text{Co}^{2+}$  ions in Cr-Zn crystal lattice. Shifting of peak position towards higher angles directly affects the lattice parameter of the samples which in turn decreases with  $\text{Co}^{2+}$  addition.



Table 1: Lattice parameter (a, c), c/a ratio, unit cell volume (V), distortion factor (u), X-ray density (d<sub>x</sub>), bulk density (d<sub>B</sub>), porosity (P) and specific surface area (S) for Co<sub>x</sub>Zn<sub>0.95-x</sub>Cr<sub>0.5</sub>O

'x'	Lattice parameter (Å)			'V' (Å) <sup>3</sup>	'u'	'd <sub>x</sub> ' (gm/cc)	'P' (%)	'S' (m <sup>2</sup> /gm)
	'a'	'c'	c/a					
0.0	3.2487	5.2043	1.602	47.599	0.379	5.635	20.50	73.0
0.02	3.2486	5.2042	1.602	47.595	0.379	5.627	21.38	68.3
0.04	3.2485	5.2041	1.602	47.591	0.379	5.618	23.47	66.3
0.06	3.2483	5.2040	1.602	47.586	0.379	5.610	25.74	65.8
0.08	3.2481	5.2038	1.602	47.579	0.379	5.601	26.13	63.4
0.1	3.2478	5.2035	1.602	47.567	0.379	5.594	28.50	62.6

Lattice constants 'a' and 'c' for hexagonal crystal geometry were evaluated by using the relations discussed elsewhere [19] which are given in Table 1. Addition of Co<sup>2+</sup> ions in Cr-Zn-O crystal lattice reduces the lattice parameter 'a' from 3.2487 to 3.2478 Å and 'c' from 5.2043 to 5.2035 Å. The decrease in lattice parameter is strongly related to the ionic radii difference of Co<sup>2+</sup> and Zn<sup>2+</sup>. Here in the present case, Co<sup>2+</sup> ions having ionic radii (0.74Å) replaces the Zn<sup>2+</sup> ions having relatively larger ionic radii (0.83Å) which in turn shrinks the lattice lengths. The constant value of c/a ratio (1.602) for all the samples confirms the hexagonal crystal geometry of the samples. Unit cell volume of the samples was estimated by using  $V = 0.866a^2c$  and the values are listed in Table 1. Decrease in lattice parameters shrinks the cell volume from 47.599 to 47.567 Å<sup>3</sup> indicating that the Co<sup>2+</sup> ions are successfully incorporated in the crystal lattice. The distortion factor 'u' for the wurtzite structure was calculated by using the following relation [20]:

$$u = \left[ \frac{a^2}{3c^2} + 0.25 \right] \tag{1}$$

As explained by Bindu et al. [21], distortion factor 'u' is estimation of the displacement of each atom along 'c' axis with respect to next atom. The estimated value of 'u' (0.379) for each sample is very close to the standard value (0.375) [20]. Mass – volume relation was used to estimate the bulk density and X-ray density was calculated by using the relation taken from literature [22]. Percentage porosity and specific surface area of all the samples were obtained by using the following relations [22]:

$$P(\%) = \left( \frac{d_x - d_B}{d_B} \right) \times 100 \tag{2}$$

$$S = \frac{6000}{td_B} \tag{3}$$

Where, d<sub>x</sub> – is the X-ray density, d<sub>B</sub> – bulk density, S – specific surface area, t – is crystallite size and d<sub>B</sub> is the bulk density. Calculated values of X-ray density, porosity and specific surface area are listed in Table 1. It can be seen that the X-ray density and percentage porosity increases while as specific surface area decreases with the addition Co<sup>2+</sup> ions in Cr-Zn crystal lattice. The XRD peak broadenings were analyzed by using W-H analysis which provides the information of size and shape of the samples. Crystallite size and lattice strain induced in the crystal lattice were computed by using the following equation which assumes the uniform deformation model (UDM) [23]:

$$\beta \cos \theta = 4\epsilon \sin \theta + \frac{k\lambda}{t_{W-H}} \tag{4}$$

Figure 2 shows the linearly fitted UDM plots drawn between 4Sinθ and βCosθ. Slopes of UDM plots gives the lattice strain induced in the crystal lattice whereas Y-intercept gives the value of average crystallite size (t). It can be seen from Table 2 that the average crystallite size obtained from UDM plots varies from 19.36 to 25.63 nm with the addition of Co<sup>2+</sup> ions. While as, positive values of lattice strain induced in the crystal lattice indicating the tensile type of strain which reduces from 2.35 × 10<sup>-4</sup> to 0.619 × 10<sup>-4</sup> with the addition of Co<sup>2+</sup> ions.

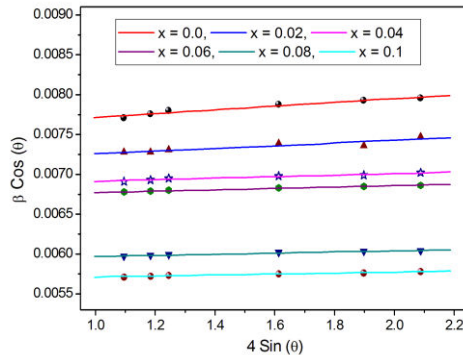


Fig. 2: W-H plots of Uniform Deformation Model for  $Co_xZn_{0.95-x}Cr_{0.05}O$  nanoparticles

Table 2: Crystallite size (t) and strain induced in  $Co_xZn_{0.95-x}Cr_{0.05}O$

'x'	W-H Analysis								SSP Method	
	UDM		USDM			UEDDM				
	't' (nm)	$\epsilon \times 10^{-4}$	't' (nm)	$\epsilon \times 10^{-4}$	$\sigma$ (MPa)	't' (nm)	$\epsilon \times 10^{-4}$	u (KJ/m <sup>3</sup> )	't' (nm)	$\epsilon \times 10^{-3}$
0.0	19.36	2.35	19.28	2.20	27.9	19.33	2.26	3.25	19.32	6.49
0.02	20.40	1.65	20.37	1.55	19.7	20.40	1.61	1.64	20.04	3.80
0.04	21.23	0.937	21.20	0.864	10.9	21.20	0.903	0.52	21.18	3.64
0.06	22.56	0.808	22.28	0.735	9.31	22.63	0.773	0.38	21.56	3.15
0.08	23.74	0.716	24.13	0.662	8.38	24.54	0.691	0.30	24.52	2.96
1.0	25.63	0.619	25.58	0.572	7.24	25.63	0.597	0.23	25.60	2.69

Microstructure of the materials has prime importance in accordance with the electrical and magnetic properties. Equation (4) is based on the isotropic nature of the samples and uniform strain induced in the crystal lattice. Uniform stress deformation model (USDM), is the another deformation model considered for the evaluation of strain and crystallite size.

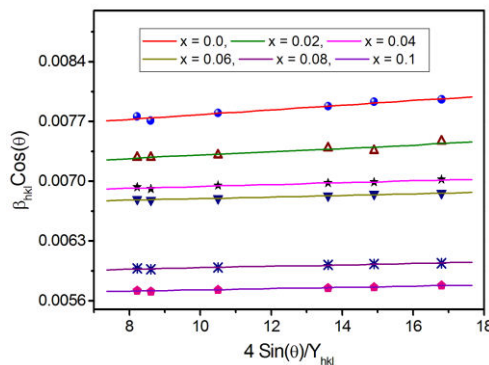


Figure 3: W-H plots of uniform stress deformation model for  $Co_xZn_{0.95-x}Cr_{0.05}O$  nanoparticles

Figure 3 shows the USDM plots drawn between  $\beta_{hkl} \cos\theta$  and  $4 \sin\theta / Y_{hkl}$  obtained by applying the Hook's law. There is linear relationship between stress and strain induced in the crystal lattice and is given by  $\epsilon = \sigma / Y$ , where  $\sigma$  - is stress and  $Y$  is Young's modulus. Hook's law modified the equation (4) as;

$$\beta \cos\theta = \sigma \left( \frac{4 \sin\theta}{Y_{hkl}} \right) + \frac{k\lambda}{t_{W-H}} \quad (5)$$

Young’s modulus  $Y_{hkl}$  is obtained from the following relation [24];

$$Y_{hkl} = \frac{\left[ h^2 + \frac{(h+2k)^2}{3} + \left(\frac{a}{c}\right)^2 \right]^2}{S_{11} \left( h^2 + \frac{(h+2k)^2}{3} \right)^2 + S_{33} \left(\frac{a}{c}\right)^4 + (2S_{13} + S_{44}) \left( h^2 + \frac{(h+2k)^2}{3} \right) \left(\frac{a}{c}\right)^2} \quad (6)$$

Stress induced in the crystal lattice was obtained from the slope of linearly fitted USDM plots shown in Figure 3 and the Y-intercept gives the values of average crystallite size of the samples. Table 2 represents the stress, strain and crystallite size obtained from USDM plots.

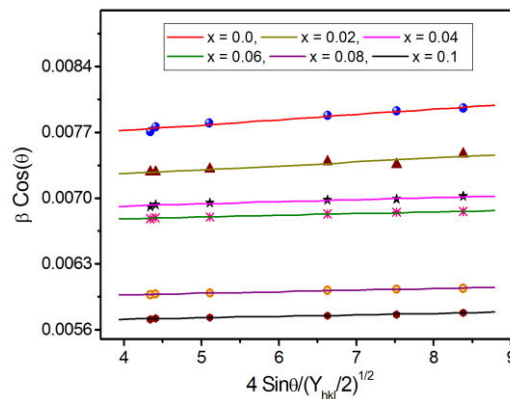


Fig. 4: W-H plots of Uniform deformation energy density model for  $Co_xZn_{0.95-x}Cr_{0.05}O$  nanoparticles

Uniform deformation energy density model (UDEDM) was assumed to evaluate the energy density of the crystals by using the relation  $u = (\epsilon^2 Y)/2$  [24]. Following equation (7) is used to estimate the lattice strain and crystallite size by using UDEDM model [23]:

$$\beta \text{Cos}\theta = \sqrt{u} \left( \frac{4 \text{Sin}\theta}{(Y_{hkl}/2)^2} \right) + \frac{k\lambda}{t_{W-H}} \quad (7)$$

Figure 4, represents the UDEDM plots drawn between  $\beta \text{Cos}\theta$  and  $4 \text{Sin}\theta / (Y_{hkl}/2)^2$ . Slope of the plots gives the root mean square values of energy density from which strain can be calculated and Y-intercept gives the values of crystallite size  $t_{W-H}$ . Both lattice strain and average crystallite size obtained from all the three models viz. UDM, USDM, UDEDM are in good agreement with each other.

W-H analysis is completely true when the line broadening is essentially isotropic which implies that the strain induced within the crystal lattice is uniformly distributed. Another method, size-strain plot method, which evaluates the size and strain by considering Lorentzian and Gaussian functions for X-ray line profile fitting [25].

$$(d\beta \text{Cos}\theta)^2 = \left(\frac{\epsilon}{2}\right)^2 + \frac{k\lambda}{t_{W-H}} (d^2 \beta \text{Cos}\theta) \quad (8)$$

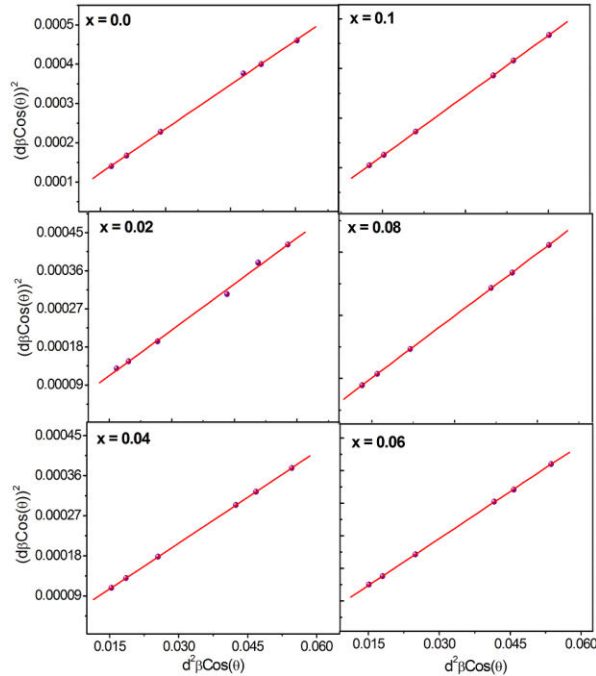
Fig 5: Strain – size plots of  $\text{Co}_x\text{Zn}_{0.95-x}\text{Cr}_{0.05}\text{O}$  nanoparticles

Figure 5 shows the size-strain plots drawn between  $(d\beta\cos\theta)^2$  and  $d^2\beta\cos\theta$ . Crystallite size and lattice strain obtained from the slopes and Y-intercept of strain-size plots are given in Table 2, which are in good agreement with the W-H analysis.

#### IV. CONCLUSIONS

Oxide nanoparticles of  $\text{Co}^{2+}$  doped Cr-Zn-O were successfully obtained by using the sol-gel auto-ignition route. Single phase hexagonal wurtzite crystal structure of all the samples was confirmed by using X-ray diffraction analysis. Bragg's peak positions shifted slightly towards higher angles which decreases lattice constants 'a' and 'c' with the substitution of  $\text{Co}^{2+}$  ions in Cr-Zn crystal lattice. W-H analysis and SSP method indicate that the tensile type strain is induced in the crystal lattice and it decreases with the increasing percentage of  $\text{Co}^{2+}$  ions. Crystallite size obtained from both W-H and SSP methods is obtained in nanometer range. Lattice strain induced in the crystal lattice obtained from SSP method ranges from  $6.49 \times 10^3$  to  $2.69 \times 10^3$  and its variation is in good agreement with the results obtained from W-H analysis.

#### REFERENCES

- [1] R. H. Kadam, A. Karim, A. B. Kadam, A. S. Gaikwad, S. E. Shirsath, Influence of  $\text{Cr}^{3+}$  substitution on the electrical and magnetic properties of  $\text{Ni}_{0.4}\text{Cu}_{0.4}\text{Zn}_{0.2}\text{Fe}_2\text{O}_4$  nanoparticles; Inter. Nano. Lett. vol. 2, No. 1, pp. 1-5, 2012.
- [2] R. Elilarassi, G. Chandrasekaran; Synthesis and optical properties of Ni-doped zinc oxide nanoparticles for optoelectronic applications; Opt. Lett. vol. 6, pp. 6-10, 2010.
- [3] R. H. Kadam, K. Desai, V. S. Shinde, M. Hashim, S. E. Shirsath; Influence of  $\text{Gd}^{3+}$  ion substitution on the  $\text{MnCrFeO}_4$  for their nanoparticles shape formation and magnetic properties; J. Alloy. Comp. vol. 657, pp. 487-494, 2016.
- [4] M. Kaur, P. Kaur, G. Kaur, K. Dev, P. Negi, R. Sharma; Structural, morphological and optical properties of Eu-N co-doped zinc oxide nanoparticles synthesized using co-precipitation technique; Vacuum, vol. 155, pp. 689-695, 2018.

- [5] Z. Joshi, D. Dhruv, K. N. Rathod, J. H. Markna, A. Satyaprasad, A. D. Joshi, P. S. Solanki, N. A. Shah; Size effects on electrical properties of sol-gel grown chromium doped zinc oxide nanoparticles; *J. Mater. Sci. Techn.* vol. 34, No. 3, pp. 488-495, 2018.
- [6] M. Vagadia, A. Ravalia, U. Khachar, P. S. Solanki, R. R. Doshi, S. Rayaprol, D. G. Kuberkar; Size and grain morphology dependent magnetic behaviour of Co doped ZnO, *Mater. Res. Bull.* vol.46, pp. 1933-1937, 2011.
- [7] R. Saleh, N. F. Djaja; Transition – metal – doped ZnO nanoparticles: Synthesis, characterization and photocatalytic activity under UV light; *Spect. Act. Part A: Mole. Bio. Spect.* vol. 130, pp.581-590, 2014.
- [8] Z. Jin, T. Fukumura, M. Kawasaki; High temperature fabrication of transition – metal – doped epitaxial ZnO thin films: A series of oxide – diluted magnetic semiconductors and their properties; *Appl. Phys. Lett.* vol. 78 Article No. 3824, 2001.
- [9] M. Vegadia, A. Ravalia, S. Katba, P. S. Solanki, K. Bapna, M. Kumar, R. J. Choudhary, D. M. Phase, D. G. Kuberkar; Co-substitution driven electronic structure modifications in  $Zn_{1-x}Co_xO$ ; *J. Alloy. Comp.* vol. 610, pp. 113-117, 2014.
- [10] R. Razali, A. K. Zak, W. A. Majid, M. Darroudi; Solvothermal synthesis of microsphere ZnO nanostructures in DEA media; *Ceram. Inter.* vol. 37, pp. 3657-3663, 2011.
- [11] S. K. Gurav, S. E. Shirsath, R. H. Kadam, S. M. Patange, K. S. Lohar, D. R. Mane; Less magnetic and larger  $Zr^{4+}$ - $Zn^{2+}$  ions co-substituted structural and magnetic properties of ordered  $Li_{0.5}Fe_{2.5}O_4$  nanoparticles; *Mater. Res. Bull.* vol. 48, pp. 3530-3536, 2013.
- [12] S. Liu, H. Sun, A. Suvorova, S. Wang; One pot hydrothermal synthesis of ZnO – reduced graphene oxide composites using Zn powders for enhanced photocatalysis, *Chem. Engg. J.* vol. 229, pp. 533-539, 2013.
- [13] S. Debnath, R. Das; Cobalt doping on nickel ferrite nanocrystals enhanced the micro – structural and magnetic properties: shows a correlation between them; *J. Alloy. Comp.* vol. 852, Article No. 156884, 2021.
- [14] S. R. Wadgane, S. T. Alone, A. Karim, G. Vats, S. E. Shirsath, R. H. Kadam; Magnetic field induced polarization and magnetoelectric effect in  $Na_{0.5}Bi_{0.5}TiO_3-Co_{0.75}Zn_{0.25}Cr_{0.2}Fe_{1.8}O_4$ ; *J. Magn. Magn. Mater.* vol. 471, pp. 388-393, 2019.
- [15] S. S. Choudhari, S. R. Wadgane, B. P. Gaikwad, S. S. Satpute, K. M. Batoo, O. M. Aldossary, S. E. Shirsath, R. H. Kadam; Strain mediated enhancement in magnetoelectric properties of sonochemically synthesized piezoelectric and piezomagnetic composites; *Ceram. Inter.* vol. 47, pp. 6496-6504, 2021.
- [16] R. Delhez, Th. Keijsers, E. J. Mittemeijer; Determination of crystallite size and lattice distortions through X-ray diffraction line profile analysis; *Fres. Zeit. Anal. Chem.* vol. 312, pp.1-16, 1982.
- [17] V. More, R. B. Borade, K. Desai, V. K. Barote, S. S. Kadam, V. S. Shinde, D. R. Kulkarni, R. H. Kadam, S. T. Alone; Site occupancy, surface morphology and mechanical properties of  $Ce^{3+}$  added Ni-Mn-Zn ferrite nanocrystals synthesized via sol-gel route; *Nano: Brief Rep. Rev.* vol. 6, Article No. 2150059, 2021.
- [18] A. B. Kadam, V. K. Mande, S. B. Kadam, R. H. Kadam, S. E. Shirsath, R. B. Borade; Influence of gadolinium ( $Gd^{3+}$ ) ion substitution on structural, magnetic and electrical properties of cobalt ferrites; *J. Alloy. Comp.* vol. 840, Article No. 155669, 2020.
- [19] S. S. Satpute, S. R. Wadgane, S. R. Kadam, D. R. Mane, R. H. Kadam;  $Y^{3+}$  substituted Sr-Hexaferrites: sol-gel synthesis, structural, magnetic and electrical characterization; vol. 65, pp. 274-281, 2019.
- [20] P. S. Sundaram, T. Sangeetha, S. Rajakarthishan, R. Vijayalakshmi, A. Elangovan, G. Arivazhagan; XRD structural studies on cobalt doped zinc oxide nanoparticles synthesized by co-precipitation method: Williamson – Hall and size – strain plot approaches; *Physica B: Cond. Mater.* vol. 595, Article No. 412342, 2020.
- [21] P. Bindu, S. Thomas; Estimation of lattice strain in ZnO nanoparticles: X-ray peak profile analysis, *J. Theor. Appl. Phys.* vol. 8, pp. 123-134, 2014.
- [22] S. S. Satpute, S. R. Wadgane, K. Desai, D. R. Mane, R. H. Kadam; Substitution effect of  $Y^{3+}$  ions on the structural, magnetic and electrical properties of cobalt ferrite nanoparticles; *Ceramica* vol. 66, pp. 4349, 2020.
- [23] K. V. Chandekar, K. M. Kant; Size-strain analysis and elastic properties of  $CoFe_2O_4$  nanoparticles by hydrothermal method; *J. Mole. Stru.* 1154 (2018) 418-427.
- [24] K. R. Desai, S. T. Alone, S. R. Wadgane, S. E. Shirsath, K. M. Batoo, A. Imran, E. H. Raslan, M. Hadi, M. F. Ijaz, R. H. Kadam; X-ray diffraction based Williamson-Hall analysis and Rietveld refinement for strain mechanism in Mg-Mn co-substituted  $CdFe_2O_4$  nanoparticles; *Physica B: Cond. Mater.* vol. 614 Article No. 413054, 2021.



**INNO**  **SPACE**  
SJIF Scientific Journal Impact Factor

**Impact Factor:  
7.512**

**ISSN** INTERNATIONAL  
STANDARD  
SERIAL  
NUMBER  
**INDIA**



# INTERNATIONAL JOURNAL OF INNOVATIVE RESEARCH

IN SCIENCE | ENGINEERING | TECHNOLOGY

 **9940 572 462**  **6381 907 438**  **ijirset@gmail.com**



[www.ijirset.com](http://www.ijirset.com)

Scan to save the contact details